



Chemical compatibility and properties of suspension plasma-sprayed SrTiO_3 -based anodes for intermediate-temperature solid oxide fuel cells

Shan-Lin Zhang, Cheng-Xin Li*, Chang-Jiu Li

State Key Laboratory for Mechanical Behavior of Materials, School of Materials Science and Engineering, Xi'an Jiaotong University, Xi'an, Shaanxi 710049, China



HIGHLIGHTS

- Nano-sized LST and SDC powders are produced for SPS.
- Ni reacted with LSGM electrolyte at or above 600 °C.
- LST exhibits a good chemical compatibility with SDC and LSGM.
- SPS was employed to prepare the LST–SDC composite anode.
- Test cell shows a power density of 221 mW cm^{-2} at 800 °C and increase by 37% with the annealed anode.

ARTICLE INFO

Article history:

Received 15 November 2013

Received in revised form

18 April 2014

Accepted 19 April 2014

Available online 30 April 2014

Keywords:

Solid oxide fuel cells

Composite anode

La-doped strontium titanate

Sm-doped ceria

Suspension plasma spraying

Chemical compatibility

ABSTRACT

La-doped strontium titanate (LST) is a promising, redox-stable perovskite material for direct hydrocarbon oxidation anodes in intermediate-temperature solid oxide fuel cells (IT-SOFCs). In this study, nano-sized LST and Sm-doped ceria (SDC) powders are produced by the sol–gel and glycine–nitrate processes, respectively. The chemical compatibility between LST and electrolyte materials is studied. A LST–SDC composite anode is prepared by suspension plasma spraying (SPS). The effects of annealing conditions on the phase structure, microstructure, and chemical stability of the LST–SDC composite anode are investigated. The results indicate that the suspension plasma-sprayed LST–SDC anode has the same phase structure as the original powders. LST exhibits a good chemical compatibility with SDC and Mg/Sr-doped lanthanum gallate (LSGM). The anode has a porosity of ~40% with a finely porous structure that provides high gas permeability and a long three-phase boundary for the anode reaction. Single cells assembled with the LST–SDC anode, $\text{La}_{0.8}\text{Sr}_{0.2}\text{Ga}_{0.8}\text{Mg}_{0.2}\text{O}_3$ electrolyte, and $\text{La}_{0.8}\text{Sr}_{0.2}\text{CoO}_3$ –SDC cathode show a good performance at 650–800 °C. The annealing reduces the impedances due to the enhancement in the bonding between the particles in the anode and interface of anode and LSGM electrolyte, thus improving the output performance of the cell.

© 2014 Elsevier B.V. All rights reserved.

1. Introduction

Solid oxide fuel cells (SOFCs) have been widely investigated as an efficient and environment-friendly alternative to conventional power generation using fossil fuels [1]. To solve severe problems during high temperature operations, such as the material selection for current collector and sealing problems, one of the major concerns is to reduce the operating temperature from 1000 °C to

<800 °C. Therefore, it is essential to use electrolytes with high ionic conductivity and electrodes with high catalytic activity for intermediate-temperature SOFCs (IT-SOFCs) [2]. Mg/Sr-doped lanthanum gallate (LSGM) is one of the representative electrolytes for applications in SOFCs at 600–800 °C owing to its high ionic conductivity and stability over a wide range of oxygen partial pressure [3–5]. However, the conventional Ni-based cermet anode materials are not suitable for LSGM electrolyte because of the interfacial reaction between the anode and electrolyte during the cell fabrication process, which results in significant performance degradation [6–9]. When the sintering temperature is >1250 °C, LSGM electrolyte reacts with NiO to produce LaNiO_3 with low

* Corresponding author. Tel.: +86 29 82660970; fax: +86 29 83237910.

E-mail address: lcx@mail.xjtu.edu.cn (C.-X. Li).

conductivity and catalytic activity. Moreover, Ni reacts with LSGM when the operation temperature is >1000 °C [10]. Until now, the long-time stability of Ni and LSGM at intermediate temperature range has not been reported. Therefore, it is desirable to develop alternative anode materials for the further development of IT-SOFCs with LSGM electrolyte. La-doped strontium titanate (LST) is one of the perovskite ceramic oxides with significantly high electronic conductivity; therefore, LST is considered suitable as anode material [11–13]. LST has a conductivity of >20 S cm $^{-1}$ at 973 K [14]. Moreover, in the SOFCs with LST anode, methane can be directly used as the fuel, and the cells exhibit high sulfur-tolerant ability [15]. Several studies showed that the cells with LSGM electrolyte and LST anode exhibit a good performance [16,17]. Further, LST has attracted much interest owing to its thermal and chemical stability with ZrO₂-based electrolyte in fuel cells operating environment [18,19].

Usually, to enhance the electrochemical performance, a composite anode of Gd or Sm-doped CeO₂ (GDC or SDC) and LST is designed [13,16,17]. For SOFC anode, a porosity of ~ 30 –40% and a uniform pore distribution are required. In addition, a long three-phase boundary (TPB) is also necessary for anode reactions. Therefore, the fabrication process of anode plays an important role in determining the performance of SOFCs and their commercial applications. Until now, several approaches have been used to fabricate SOFCs electrodes, such as sol–gel method [20], tape-casting [21], screen-printing [22], and plasma spraying [23–25]. Compared to other methods, plasma spraying is one of the cost-effective methods owing to its fast deposition rate and easy automation features. In particular, for tubular and other complex geometrical SOFCs, plasma spraying shows a high flexibility during the electrode fabrication process. As one of the variations of plasma spraying technologies, suspension plasma spraying (SPS) can be used to deposit ceramic coatings with fine grains from sub-micrometers to nanometers. The size of splats in the deposits is usually one to two orders of magnitude smaller than that deposited by conventional plasma spraying, thus providing more TPB advantageous for SOFCs electrode applications [26]. Moreover, homogeneously distributed components are expected in the fabricated coatings because of the homogeneity of the suspension. In summary, the SPS process has great potential to fabricate a highly efficient anode.

Until now, LST-based composite anodes were mainly prepared by slurry coating [13] and screen printing methods [17]. To the best of our knowledge, there are no published reports describing the use of plasma spraying to prepare LST-based anodes. The purpose of this study was to fabricate an LST–SDC composite anode by the SPS method and investigate the microstructure of the composite anode and its effect on the anode performance. In this study, nano-sized LST and SDC powders that are suitable for SPS were prepared. The chemical compatibility between LST, LSGM, and SDC was studied. Moreover, the reaction of Ni anode with LSGM electrolyte at intermediate temperature was also investigated. The effects of the annealing treatment on the microstructure and electrochemical performance of the composite anode were evaluated.

2. Experimental

2.1. Synthesis and powder characterization

In this study, 20% La-doped SrTiO₃ (La_{0.2}Sr_{0.8}TiO₃) powders were prepared by the sol–gel method. La(NO₃)₃·6H₂O (99.99%, Sino-pharm Chemical Reagent Co., Ltd (SCRC), China), SrCl₂·6H₂O (99.99%, SCRC), and TiCl₄ (99.9%, SCRC) were used as the starting materials. Stoichiometric amounts of La(NO₃)₃·6H₂O and SrCl₂·6H₂O were dissolved in deionized water to prepare a nitrate

Table 1
Suspension plasma spray parameters for LST–SDC composite anode.

Parameter	Unit	Value
Plasma arc power	kW	36
Arc voltage	V	60
Arc current	A	600
Flow rate of primary gas (Ar)	slpm	50
Flow rate of secondary gas (H ₂)	slpm	4.5
Suspension feed rate	ml min $^{-1}$	50
Deposition temperature	°C	400–600
Spray distance	mm	80

and chloride mixture, namely, solution A. A stoichiometric amount of TiCl₄ was dissolved in dehydrated alcohol (99.7%, Ante) to make an alcoholic solution, namely, solution B. Solutions A and B were mixed and stirred to form a uniform mixture. Citric acid and ethylene glycol (EG, HOCH₂CH₂OH, 99.8%, SCRC) were added to the solution. The molar ratio of EG and citric acid to metal was 1.5:1 and 2:1, respectively. The pH of the resulting solution was adjusted to 2–3 with appropriate quantities of NH₃·H₂O. The homogeneous solution was heated on a water bath at 80 °C. After the evaporation of water and alcohol, a viscous gel of metal–citrate complex was obtained. The viscous gel was dried at 150 °C to afford a foam-like dried gel. The conversion of the dried gel to ceramic powder was analyzed using a thermogravimetric/differential thermal analysis system (NETZSCH model STA 449C). The dried gel was heated from room temperature to 1000 °C at a heating rate of 10 °C min $^{-1}$ in air. Based on the thermal analysis results, the gel was calcined in air between 600 and 1200 °C for 3 h to produce the LST powders.

20% Sm-doped CeO₂ (Sm_{0.2}Ce_{0.8}O₂) powders were prepared by the glycine–nitrate process (GNP). Ce(NO₃)₃·6H₂O (99.99%, SCRC) and Sm(NO₃)₂·6H₂O (99.99%, SCRC) were used as the starting materials. Stoichiometric amounts of Ce(NO₃)₃·6H₂O and Sm(NO₃)₂·6H₂O were dissolved in deionized water to prepare a nitrate solution. Glycine (NH₂CH₂COOH, 99.9%, SCRC) was added to the solution as the fuel. The molar ratio of glycine to metal was maintained at 1.5:1. After stirring the solution at 80 °C for 1 h, the water was evaporated till dryness. After drying, the mixture was heated up to ~ 200 °C. Then, the combustion reaction occurred within a few minutes to afford the primary powder. The as-synthesized powder was calcined at 800 °C for 3 h. The phase structures of the LST and SDC powders were estimated by X-ray diffraction (XRD) analysis (Xpert PRO, PANalytical, Netherlands). The morphologies of LST and SDC powders were observed by scanning electron microscopy (SEM, TESCAN MIRA 3 LMH, Czech).

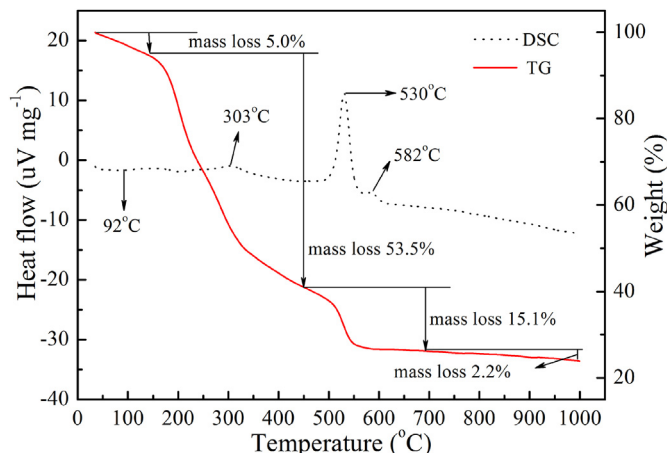


Fig. 1. DSC–TG curves for LST-dried gel precursor.

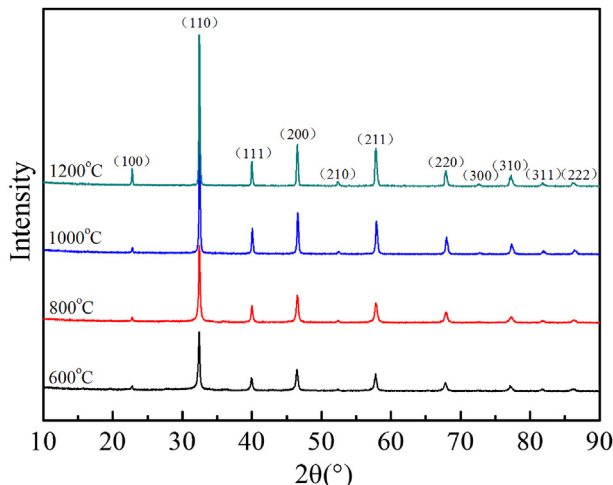


Fig. 2. XRD patterns of the LST gel precursors calcined at different temperatures.

2.2. Study of chemical compatibility

The chemical compatibility between the anodes and electrolytes under different atmospheres was investigated by XRD measurements. First, the chemical compatibility between the conventional Ni anode and LSGM electrolyte was studied. NiO powders (Shudu nano materials Co., Ltd, Chengdu, China, $<5\text{ }\mu\text{m}$) and LSGM powders ($\text{La}_{0.8}\text{Sr}_{0.2}\text{Ga}_{0.8}\text{Mg}_{0.2}\text{O}_3$, Toshima MFG Co., Ltd., Japan, $<10\text{ }\mu\text{m}$) were mixed in a 1:1 mass ratio in an agate mortar and then pressed into pellets with a diameter of 20 mm at 150 MPa. The pellets were reduced in H_2 at $550\text{ }^\circ\text{C}$ for 3 h. Then, the reduced pellets were fired in $\text{H}_2 + 3\% \text{H}_2\text{O}$ between 550 and $800\text{ }^\circ\text{C}$ to evaluate the reaction and stability between Ni and LSGM. Then, the compatibility between LST and both the electrolyte materials, LSGM and SDC, was

also investigated. The LST and electrolytes powders were mixed in a 1:1 mass ratio in an agate mortar and then pressed into pellets with a diameter of 20 mm at 150 MPa. One pellet was sintered in air at $1450\text{ }^\circ\text{C}$ for 10 h, and the other pellets were calcined at $1050\text{ }^\circ\text{C}$ for 10 h in different atmospheres, $\text{H}_2 + 3\% \text{H}_2\text{O}$, $\text{CO}_2 + 3\% \text{H}_2\text{O}$, and $\text{CH}_4 + 3\% \text{H}_2\text{O}$.

2.3. Preparation and characterization of suspension plasma-sprayed LST–SDC anode

To prepare the LST–SDC suspension for plasma spraying, the LST and SDC powders were ball milled in a 1:1 weight ratio (volume ratio $\sim 5.5:4.5$) in ethanol for 5 h. Then, the concentration of the solid particles in the resulting suspension was diluted to 0.05 mol L^{-1} by ethanol. The plasma spraying was performed in atmosphere using a conventional plasma spray system (GDP-80, 80 kW class, Jiujiang, China). The suspension was injected into the plasma jet using a liquid injector. The spray parameters are listed in Table 1. To investigate the effects of the annealing on the deposit microstructure, the deposits were annealed in air at $1250\text{ }^\circ\text{C}$ and $1350\text{ }^\circ\text{C}$ for 5 h. The phase composition of the deposits was estimated based on the XRD analysis. The microstructure of the deposits was characterized by SEM.

2.4. Fabrication and characterization of SOFC single cells

In this study, the SOFC single cells for test were supported by LSGM electrolyte. LSGM powders ($<10\text{ }\mu\text{m}$) were pressed into pellets with a diameter of 25 mm at 100 MPa. The pellets were sintered at $1550\text{ }^\circ\text{C}$ for 10 h. After polishing, dense electrolyte pellets with a diameter of 22 mm and a thickness of $\sim 300\text{--}350\text{ }\mu\text{m}$ were obtained. The LST–SDC anode was deposited on the electrolyte with a thickness of $\sim 40\text{--}50\text{ }\mu\text{m}$ by SPS. To investigate the effect of the annealing on the anode performance, the anode/electrolyte was calcined at $1250\text{ }^\circ\text{C}$ for 5 h. The $\text{La}_{0.8}\text{Sr}_{0.2}\text{CoO}_3$ –SDC

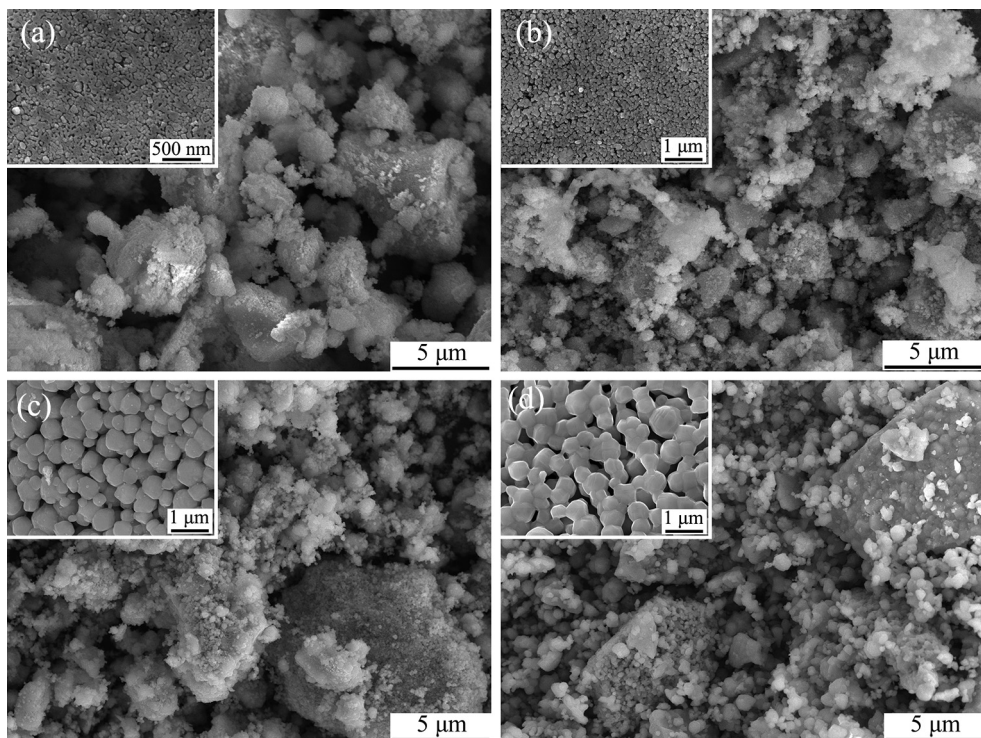


Fig. 3. Surface morphologies of LST gel precursors calcined at different temperatures: (a) $600\text{ }^\circ\text{C}$; (b) $800\text{ }^\circ\text{C}$; (c) $1000\text{ }^\circ\text{C}$ and (d) $1200\text{ }^\circ\text{C}$.

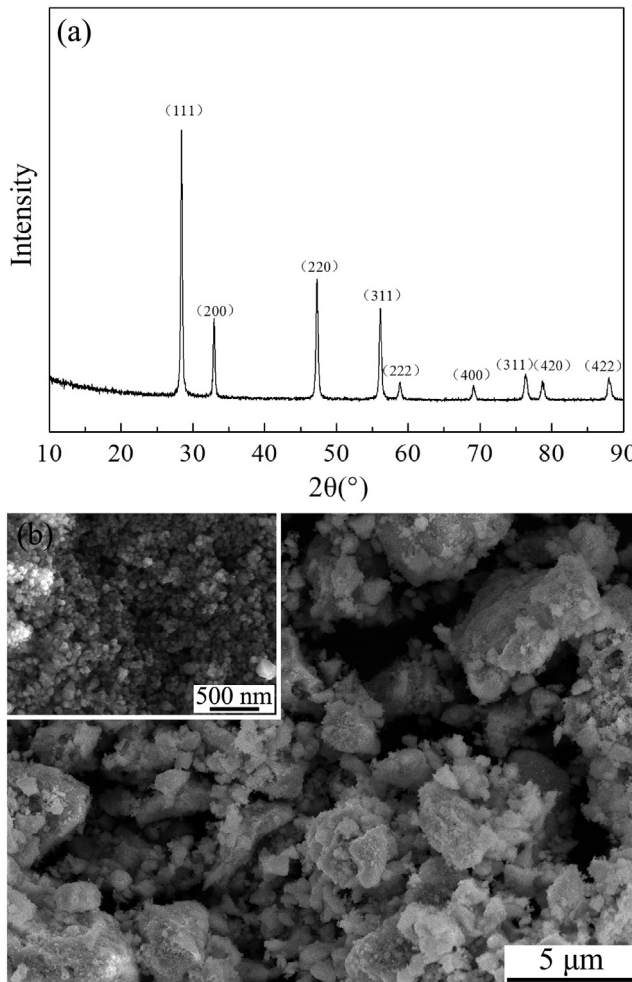


Fig. 4. XRD patterns (a) and surface morphologies (b) of SDC powders calcined at 800 °C for 3 h.

(1:1 weight ratio) composite cathode (LSC–SDC) layers were prepared on an area of 0.8 cm² with a thickness of 20–30 μm by the slurry coating method (sintered at 1000 °C for 2 h). Then, silver layers connected to two platinum wires were attached to the electrode layers for current collection via a silver paste.

The performance of the single cell was tested in a furnace with a heating and cooling rate of 3 °C min⁻¹. Before the test, the anodes were reduced in H₂ atmosphere at 800 °C for 2 h; the output performance of the cells (*I*–*V* and *I*–*P* curves) was measured in the temperature range 650–800 °C. H₂ + 3% H₂O was used as the fuel at a flow rate of 150 mL min⁻¹. The cathode side was supplied by dry O₂ at a flow rate of 200 mL min⁻¹. The electrochemical properties of the cell were tested by AC impedance spectroscopy (Solartron SI 1260/1287). The impedance spectra were obtained in the frequency range 0.1–100 KHz with applied AC voltage amplitude of 25 mV. The microstructure of the cells was characterized by SEM.

3. Results and discussion

3.1. Thermal behavior of LST gel precursor

The differential scanning calorimetry (DSC) and thermogravimetry (TG) curves for the LST foam-like dried gel are shown in Fig. 1. The DSC curve shows a weak endothermic peak at ~92 °C, which can be attributed to the volatilization of free water in the gel, leading to a mass loss of 5.0% between 50 °C and 150 °C. Between

150 °C and 450 °C, the TG curve showed a mass loss of 53.5%, which can be attributed to the redox reaction between nitrates, a part of chlorides, and citric acid; thus, an exothermic peak was observed at ~302.8 °C. Between 450 °C and 600 °C, a mass loss of 15.1% occurred accompanied by a strong exothermic peak at 530 °C on the DSC curve, which can be attributed to further combustion of the remaining organic material. A weak exothermic peak was observed at 580 °C for the combustion of residual chlorides because chlorides have a higher decomposition temperature than nitrates and citric acid. After the completion of these exothermic processes, no further major thermal events occurred up to a temperature of 1000 °C. The TG curve gradually leveled off above 600 °C, and only a 2.2% mass loss was observed between 600 and 1000 °C, which can be attributed to the dissociation of oxygen from the crystal lattice. The above mentioned thermal behavior confirms that the majority of the mass loss occurred below 600 °C, indicating that the LST was obtained from the dried gel precursor below 600 °C in this study.

3.2. Structure and morphology of LST and SDC powders

Fig. 2 shows the XRD patterns of the LST gel precursors, which were calcined for 3 h at different temperatures. According to the thermal analysis result, 600 °C was selected as the lowest calcination temperature in this study. Fig. 2 shows that the LST gel precursors calcined in air from 600 °C to 1200 °C for 3 h exhibited a single phase of perovskite structure, which is similar to the standard XRD pattern of undoped SrTiO₃ (PDF35-0734), and no other undesired impure phase was observed. Moreover, the extent of crystallization increased with increasing calcination temperature. Thus, LST powders with a perovskite structure can be synthesized by the method used in this study.

Fig. 3 shows the surface morphologies of the LST powders calcined at different temperatures. Clearly, the calcination temperature significantly affects the morphologies and particle sizes of the powders. The low magnification images in Fig. 3(a)–(c) show that the powders calcined below 1000 °C have a flocculent structure with dispersed fine particles. However, when the calcination temperature was increased to 1200 °C, the image in Fig. 3(d) shows that the powders have a regiment massive structure. As shown in the inset of Fig. 3(a), the calcination at 600 °C afforded fine particles with an average size of ~60 nm. The inset of Fig. 3(b) and (c) shows that the mean diameters of the particles increased to ~100 and 500 nm after the calcination at 800 and 1000 °C, respectively.

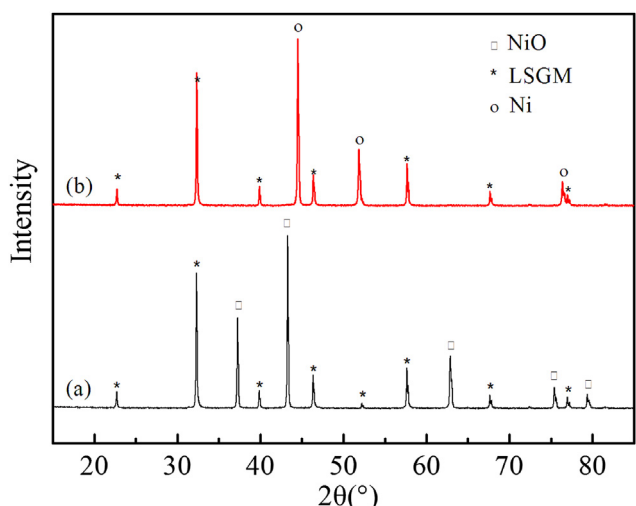


Fig. 5. XRD patterns of NiO–LSGM pellets at the original green body (a) and reduced in H₂ at 550 °C for 3 h (b).

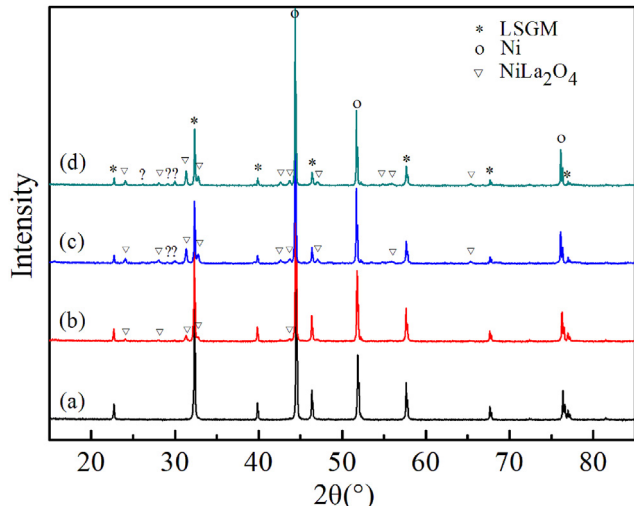


Fig. 6. XRD patterns of Ni–LSGM composites calcined in H_2 under different conditions: (a) 550 °C for 24 h, (b) 600 °C for 20 h, (c) 700 °C for 3 h, and (d) 800 °C for 3 h.

Moreover, the inset of Fig. 3(d) shows that the sintering process started by the inter-aggregation of the fine particles when the powder was calcined at 1200 °C. Fig. 4(a) shows the XRD pattern of the SDC powder calcined at 800 °C for 3 h. The powder exhibits a single phase of a cubic fluorite structure. As shown in Fig. 4(b), the SDC powder also shows a flocculent structure, and the fine spherical particles in the powder has a diameter of ~80–120 nm.

During the SPS process, the suspension should have a low viscosity, and the fine particles should be dispersed homogeneously in the solvent. Preferably, the powders should have a fine particle size with a narrow size distribution. Therefore, the LST powder calcined at 800 °C, which has a similar diameter with the SDC powder, was selected in this study as the feedstock to prepare the suspension for SPS.

3.3. Chemical compatibility of LST and reaction between Ni and LSGM electrolyte

The reactivity of the electrolytes with the anode layers is an important issue to be considered in SOFCs, because the formation of

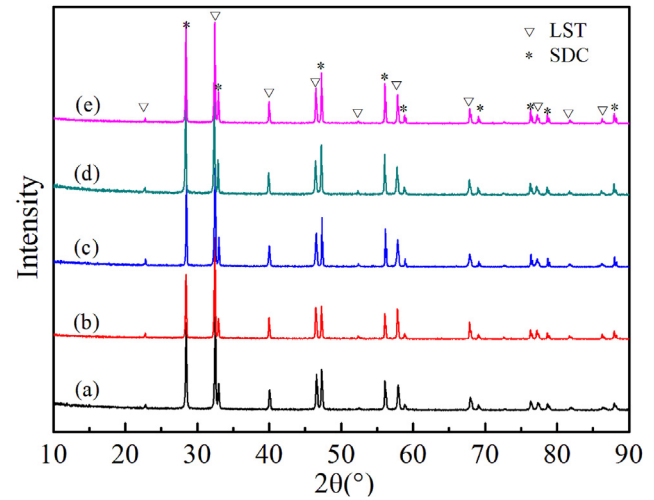


Fig. 8. XRD patterns for LST–SDC original powders (a) and for LST–SDC composite anodes sintered under different conditions: (b) sintered in air at 1450 °C for 10 h, (c) calcined in $H_2 + 3\% H_2O$ at 1050 °C for 10 h, (d) calcined in $CO_2 + 3\% H_2O$ at 1050 °C for 10 h, and (e) calcined in $CH_4 + 3\% H_2O$ at 1050 °C for 10 h.

new phases with a low ionic conductivity at the interface between the materials will significantly increase the ohmic resistance of the cell and partially block the oxygen transport. On the other hand, a poor electrode adherence may result in a large contact resistance and even delamination at the interface. Therefore, it is essential to understand the chemical compatibility between anode and electrolyte materials.

In this study, the chemical compatibility between the conventional Ni anode and LSGM electrolyte was investigated first. As shown in Fig. 5, the XRD analysis result indicates that the NiO in the NiO–LSGM pellet was reduced to Ni in H_2 at 550 °C for 3 h, and no other phase was observed, indicating that the pellet reduced at 550 °C for 3 h was composed of Ni and LSGM. Therefore, the reduced pellet can be used to study the chemical compatibility of Ni and LSGM. Fig. 6 shows the XRD patterns of the Ni–LSGM composites calcined in H_2 at different temperatures. The phase remained unchanged when the pellet was calcined at 550 °C for additional 21 h. However, a NiLa₂O₄ phase was observed when the pellet was calcined at 600 °C for 20 h. With increasing calcination temperature, the intensity of the above impurity phase became

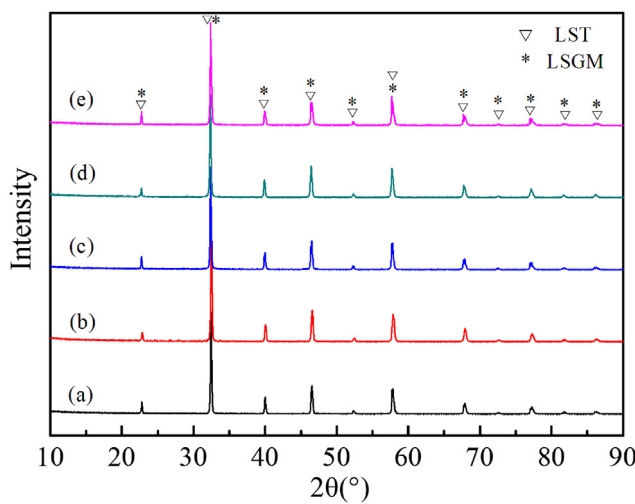


Fig. 7. XRD patterns for LST–LSGM pellets with original powders (a) and the LST–LSGM composites sintered under different conditions: (b) sintered in air at 1450 °C for 10 h, (c) calcined in $H_2 + 3\% H_2O$ at 1050 °C for 10 h, (d) calcined in $CO_2 + 3\% H_2O$ at 1050 °C for 10 h, and (e) calcined in $CH_4 + 3\% H_2O$ at 1050 °C for 10 h.

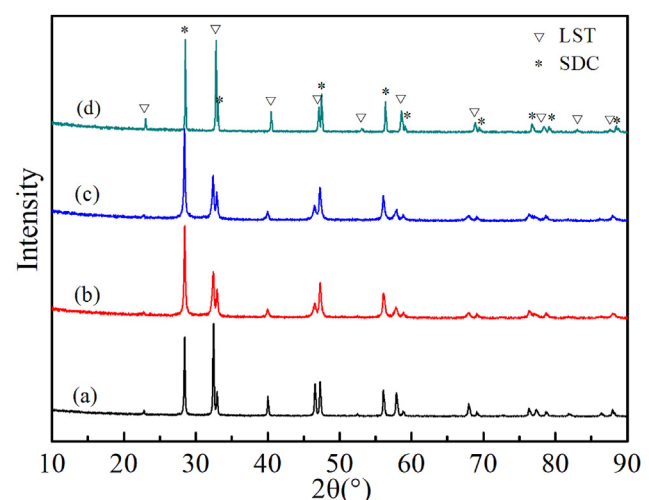


Fig. 9. XRD patterns of LST–SDC anodes compared to that of (a) spraying powders, (b) as-sprayed anode, (c) annealed in air at 1250 °C for 5 h, and (d) annealed in air at 1350 °C for 5 h.

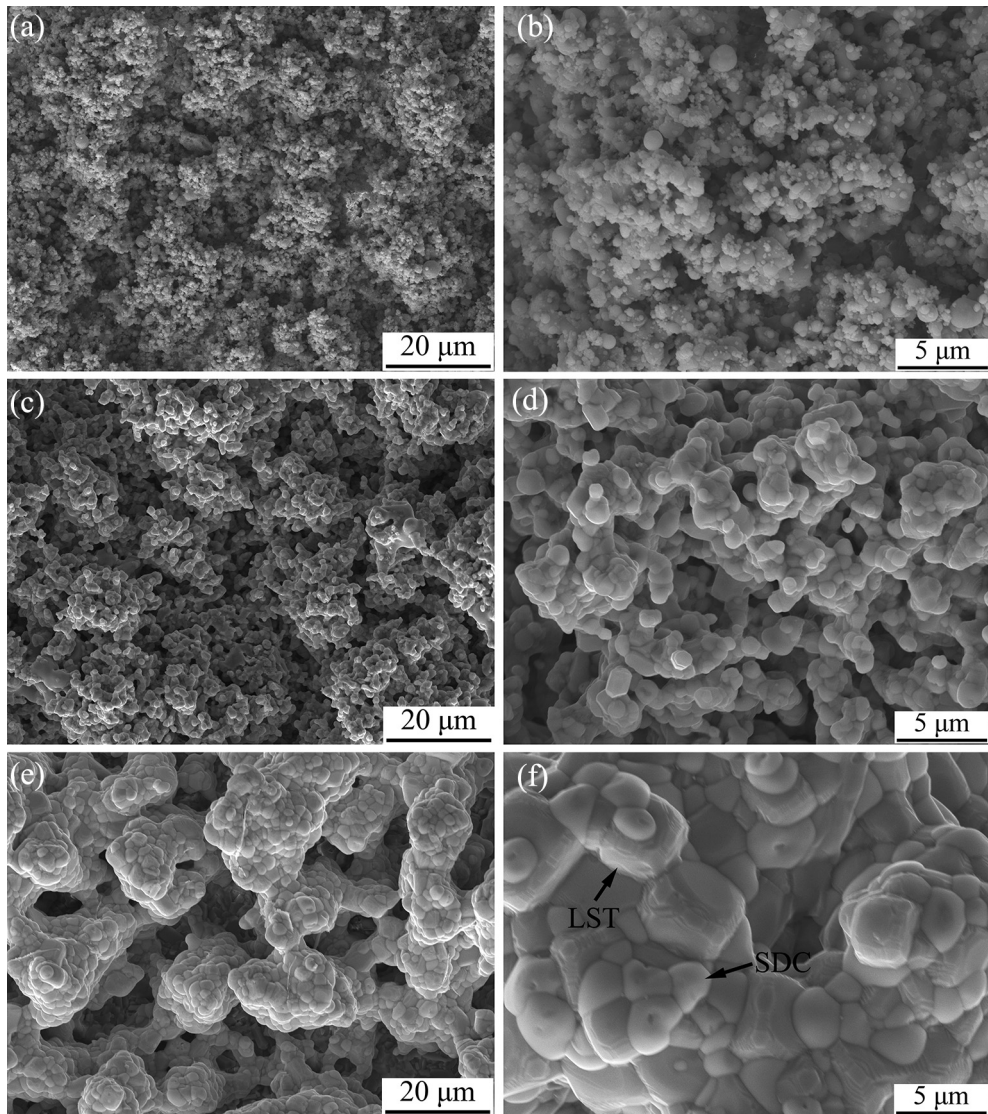


Fig. 10. Surface morphologies of LST–SDC composite anode (a) and (b) as-sprayed anode; (c) and (d) annealed in air at 1250 °C for 5 h; (e) and (f) annealed in air at 1350 °C for 5 h; (a), (c), and (e) are low magnification; (b), (d), and (f) are high magnification.

stronger. Fig. 6(c) and (d) shows that the diffraction peaks from the unidentified impurity phases (as indicated by question marks) besides the characteristic peaks of NiLa_2O_4 were observed when the pellets were calcined at 700–800 °C for 3 h.

Ni is the most widely used anode material in SOFCs and has a good chemical stability with the conventional zirconia-based electrolytes even at a high temperature above 1000 °C. However, several studies indicated that LSGM electrolyte reacted with NiO and generated the impurity phase of LaNiO_3 during the cell fabrication process when the sintering temperature was above 1250 °C [6,7,27,28]. Hwang et al. [10] reported that the reaction of LSGM electrolyte with Ni anode above 1000 °C decrease the performance during the cell operation. When the operation temperature is below 1000 °C, the cell showed a good performance. Because the long-time stability of the cell at intermediate temperature has not been reported yet, until now, several studies considered Ni as a suitable anode material for the IT-SOFCs with LSGM electrolyte. Therefore, when LSGM was used as the electrolyte, Ni was used to modify the anode in order to improve the electrical conductivity and catalytic activities [16,17,29]. However, in this study, a NiLa_2O_4 phase was observed in the Ni–LSGM composites calcined at or

above 600 °C. The La–nickel oxide formed at the interface between the LSGM electrolyte and Ni anode significantly increases the resistivity and subsequently decreases the cell performance remarkably. Therefore, this result indicates that the Ni anode is not suitable for use in LSGM electrolyte above 600 °C. Instead, the use of other proper anode materials is necessary for the IT-SOFCs with LSGM electrolyte.

Fig. 7 shows the XRD patterns of LSGM–LST pellets calcined at different temperatures and in different atmospheres. Because both LST and LSGM have a perovskite-type crystal structure, the diffraction peaks from the two materials approximately overlap as shown by the XRD patterns of the pellet without heat treatment (Fig. 7(a)). The XRD analysis results show that the sample sintered in air at 1450 °C for 10 h has a similar XRD pattern with that of the starting pellet (Fig. 7(a)). Moreover, when the pellets were calcined at 1050 °C for 10 h in the atmospheres, including $\text{H}_2 + 3\% \text{H}_2\text{O}$ (Fig. 7(c)), $\text{CO}_2 + 3\% \text{H}_2\text{O}$ (Fig. 7(d)), and $\text{CH}_4 + 3\% \text{H}_2\text{O}$ (Fig. 7(e)), it was observed that the XRD patterns are also similar to that of the starting pellet. Although the XRD diffraction peaks of both the materials overlapped and became difficult to identify the individual phases, any peaks from other phases were not observed except the

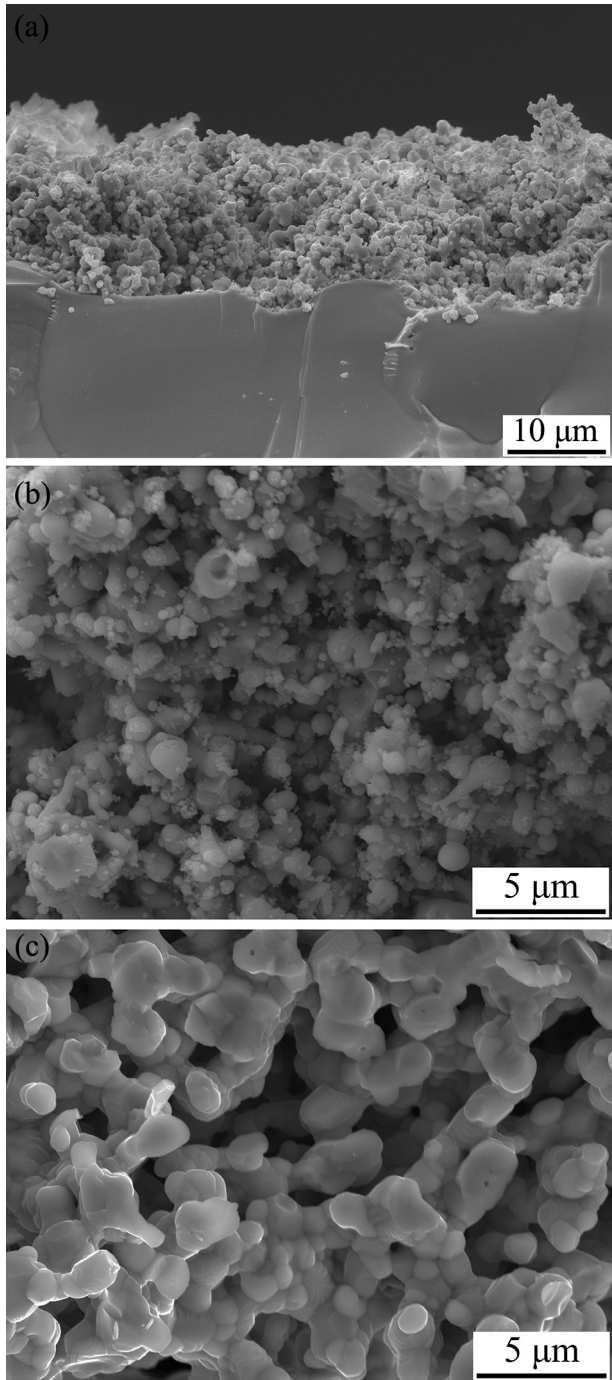


Fig. 11. Microstructure of the fractured LST–SDC composite anode: (a) as-sprayed anode on LSGM electrolyte, (b) as-sprayed anode in high magnification, (c) annealed at 1250 °C for 5 h.

characteristic peaks of LSGM and LST. Moreover, the diffraction peaks corresponding to possible reaction products were not detected. These results indicate that no reactions occurred between LST and LSGM at the above mentioned calcination conditions. Therefore, the LST has excellent chemical compatibility with LSGM as an anode material.

SDC is usually used as composite anodes in SOFCs because of its high ionic and electrical conductivities in reduction atmosphere [30–32]. Moreover, it is also applied as an interlayer to prevent the reaction between the LSGM electrolyte and anode materials [33]. Therefore, the chemical compatibility between LST and SDC is very

important. To investigate the feasibility of LST–SDC composite as the anode material, the chemical compatibility between LST and SDC was also investigated under the same conditions as those for LST and LSGM. The XRD patterns (Fig. 8) showed no peaks from any other phases except the characteristic peaks of SDC and LST under all the above mentioned conditions. These results indicate that LST has a good chemical compatibility with SDC.

3.4. Microstructure of suspension plasma sprayed LST–SDC anode

Fig. 9 shows the XRD patterns of the as-sprayed LST–SDC composite anode and those annealed at two different conditions compared to that of the starting powder. The as-sprayed LST–SDC composite anode shows the same phase structure as that of the spray powder. This result indicates that no reaction or decomposition occurred during the SPS process. Based on the XRD patterns shown in Fig. 9(c) and (d), after the composite anodes were annealed in air at 1250 °C and 1350 °C for 5 h, they have the same phase compositions as those of the pellets calcined at a high temperature. Therefore, clearly the SPS LST–SDC composite anode is chemically stable. Moreover, the extent of crystallization increased with increasing annealing temperature.

Fig. 10 shows the surface morphologies of the LST–SDC composite anodes. It can be seen from Fig. 10(a) that the surface of the as-sprayed anode has a rough and porous island-like structure. A close examination (Fig. 10(b)) clearly shows that the anode was composed by the agglomerates of spherical particles with a size $<2 \mu\text{m}$. During the SPS process, after the suspension was injected into the plasma jet, it was atomized to form suspension droplets with a size of $\sim 0.3\text{--}6 \mu\text{m}$ [34]. After the solvent was evaporated, the agglomerates of the nanoparticles formed the droplets. Then, the agglomerates were heated and simultaneously accelerated by the plasma jet to form a molten or semi-molten droplet stream with a high velocity, which projected towards a substrate to form deposits. Because the suspension droplets have different diameters, the agglomerates of spherical particles with different sizes evolved in the deposits. The flattened particles indicate that such particles melted to a certain extent prior to the impact on the substrate. On the other hand, the spherical particles well aggregated on the flattened particles, indicating that these particles were in a semi-molten state. Moreover, some small spherical particles with a size of $\sim 100\text{--}200 \text{ nm}$ adhered to the surface possibly because such melted particles cooled down before reaching the substrate due to their small size and adhered to the deposits [35]. Fig. 10(c) and (d) shows the surface morphologies of the LST–SDC composite anode annealed in air at 1250 °C for 5 h. After the annealing, the deposit also showed a rough and porous surface. The fine particles were sintered together and aggregated to form large particles with a size of $\sim 1\text{--}2 \mu\text{m}$. The good bonding among the particles increased the electrical conductivity and catalytic activity of the composite anode. Moreover, when the annealing temperature was raised to 1350 °C, the sintering of the composite anode proceeded further. Many large caves that penetrated deeply into the deposit to form pores were present on the surface (Fig. 10(e)). The formation of such caves can be attributed to the volume shrinkage effect during the sintering. The small particles aggregated to form an island-like structure. The high magnification image (Fig. 10(f)) shows that the particles have a size of $\sim 2\text{--}6 \mu\text{m}$. The LST and SDC particles can be clearly distinguished by the difference in their surface morphologies as shown in Fig. 10(f). The LST particles have a bigger size and conchoidal surface, while the SDC particles have a smaller size and smooth surface. As the SOFC anodes, the long TPB is essential. Although a high temperature sintering can enhance the particle interface bonding and subsequently enhance the electrical conductivity, the TPB of the anode may decrease with increasing

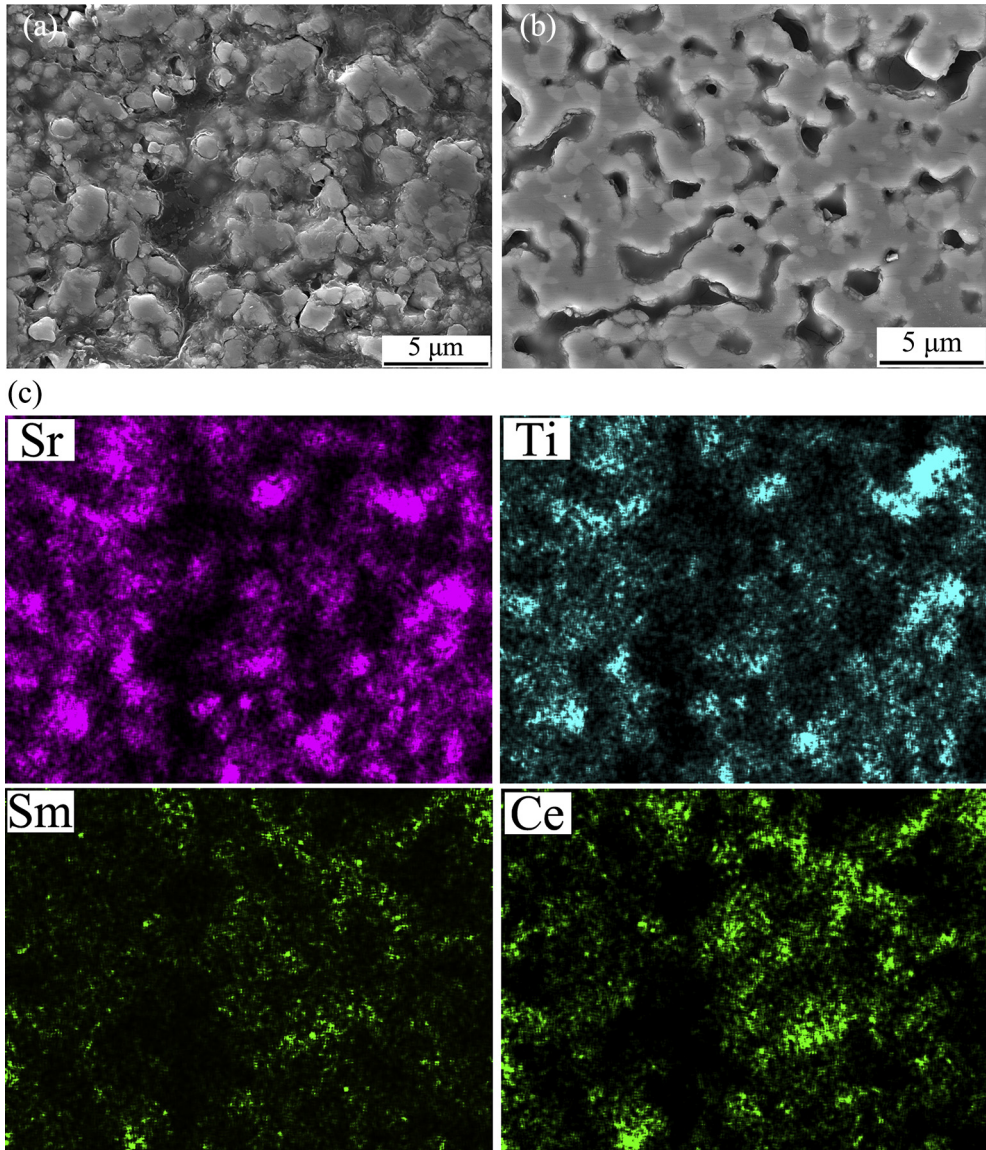


Fig. 12. Microstructure of the polished cross-section of the LST–SDC: (a) as-sprayed composite anode, (b) the anode annealed at 1250 °C for 5 h, (c) and (d) are the corresponding EDX elemental mapping images for (a) and (b).

particle size and decreasing amount of small pores. Therefore, in this study, 1250 °C was selected as the temperature for annealing the composite anodes in the preparation of SOFCs.

Fig. 11(a) shows the microstructure of the fractured LST–SDC composite anode on the LSGM electrolyte. The fracture in the as-sprayed anode apparently occurred mainly at the particle interfaces as shown in Fig. 11(b) because the interface bonding between the particles was weak. Clearly, many small particles were attached to the surface of large particles on the fracture surface. However, after the deposit was annealed at 1250 °C for 5 h (Fig. 11(c)), small particles aggregated to form the large particles because of the sintering, which apparently enhanced the interface bonding between the particles. Evidently, the larger pores evolved owing to the volume shrinkage and aggregation of fine particles during the sintering.

The microstructures of the polished cross-section of the composite anodes are shown in Fig. 12. To prevent the particles in the porous anodes from pull-out during the metallographic sample preparation, the anodes were infiltrated with epoxy adhesives by vacuum infiltration. Based on the distribution of the infiltrated

adhesives throughout the deposit, it was found that the as-sprayed anode (Fig. 12(a)) has a porosity of ~38–40 vol.%. Most of the pores were present in the anode as stacking gaps between the particles and have a size of ~1–2 μm. The pores in the annealed anode (Fig. 12(b)) were confirmed to be interconnected throughout the deposit. Moreover, the pores have a size of ~2–7 μm. The annealed anode has a porosity of ~32–35 vol.%. The slight decrease in the porosity occurred because the small pores disappeared during the annealing process. Fig. 12(c) and (d) shows the elemental distribution within both the as-deposited and annealed anodes, respectively. The energy dispersive X-ray (EDX) elemental composition indicated that the LST and SDC were uniformly distributed in the anode. Moreover, after the annealing, the distribution of LST and SDC became more uniform. This result can be attributed to the sintering-induced enhancement in the particle cohesion. The EDX measurements afforded a LST to SDC weight ratio of ~1:0.94 in the anodes, which is very close to that of the starting powders in the spray suspension. Compared to the starting powders, the slight decrease in the SDC content in the deposits can be attributed to the higher melting point than LST, ~400–500 °C.

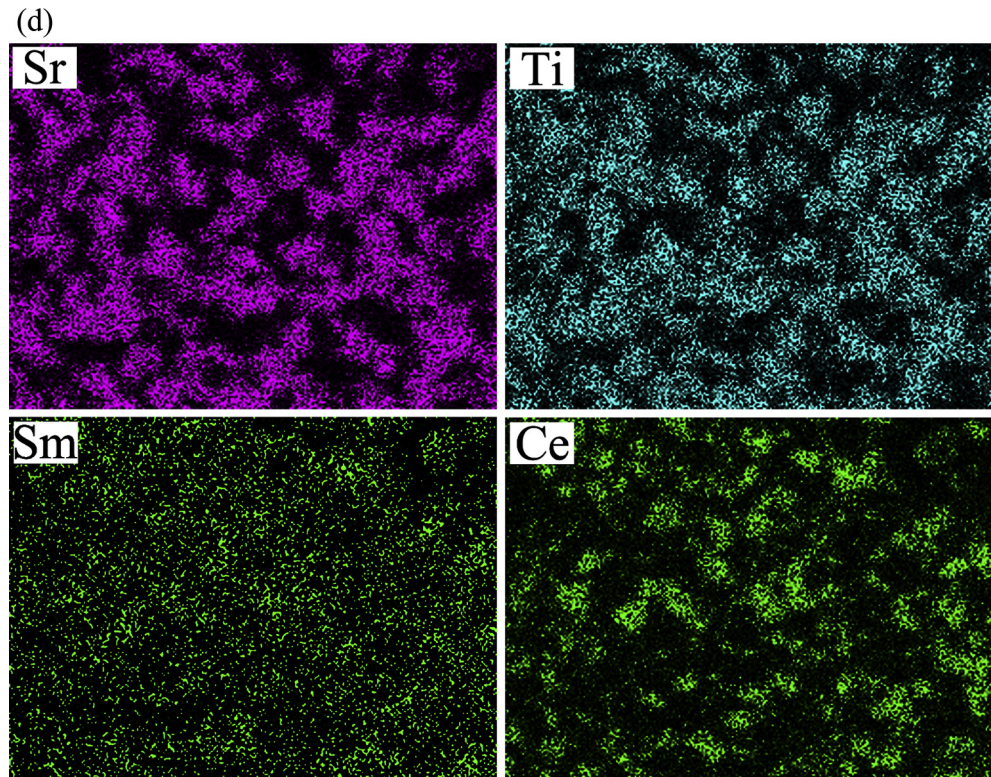


Fig. 12. (continued).

3.5. Electrochemical performance of single SOFC assembled with LST–SDC composite anode

Fig. 13(a) shows the cross-sectional structure of a SOFC single cell. The cell is based on LSGM electrolyte support. Thus, the LSGM electrolyte has a thickness of ~ 300 μm . Some closed pores are present in the electrolyte because it is difficult to sinter LSGM to make it fully dense [36,37]. The LSC–SDC composite cathode was prepared on the other side of the LSGM electrolyte by the slurry coating process to a thickness of 25 μm . The LST–SDC anode with a thickness of 40 μm was deposited on one side of the LSGM electrolyte by SPS, and one of the composite anodes was annealed at 1250 $^{\circ}\text{C}$. Then, Ag current collector layers of 15- μm thick were applied to both the anode and cathode. Both the electrodes and Ag layers showed a porous structure. Although the as-SPSed LST–SDC anode was weakly adhered to the electrolyte as shown in Fig. 13(b), after the post-spray annealing, the anode adhered well to the electrolyte (Fig. 13(c)).

The test results for the output performance of the cells are shown in Fig. 14. The cell voltage decreased nearly linearly with increasing current density at all the operating temperatures. At an operating temperature of 650 $^{\circ}\text{C}$, the cell with the as-sprayed anode (Fig. 14(a)) showed the maximum power density of 51 mW cm^{-2} . When the operating temperature was increased to 700, 750, and 800 $^{\circ}\text{C}$, the maximum power densities of the cell increased to 86, 140, and 221 mW cm^{-2} , respectively. Moreover, clearly after the anode was annealed at 1250 $^{\circ}\text{C}$ for 5 h, the cell performance improved (Fig. 14(b)). At 650 $^{\circ}\text{C}$, the cell with the annealed anode showed a maximum power density of 65 mW cm^{-2} , which increased by a factor of $\sim 27\%$. When the cell was operated at 700, 750, and 800 $^{\circ}\text{C}$, the maximum power densities increased to 110, 187, and 301 mW cm^{-2} , respectively. At 800 $^{\circ}\text{C}$, the power density increased by a factor of $\sim 37\%$ compared to the cell assembled with the as-deposited anode.

Sun et al. reported that the cell with LST–CeO₂ (1:1 wt.%) composite anode and 300- μm yttria-stabilized zirconia (YSZ) electrolyte exhibited a maximum power density of 175 mW cm^{-2} at 900 $^{\circ}\text{C}$ [38]. Kyung Bin Yoo et al. reported that the cell with 500- μm LSGM electrolyte and Ni-impregnated (1 mg cm^{-2}) LST–GDC (Gd-doped ceria) composite anode showed a maximum power density of 275 mW cm^{-2} at 800 $^{\circ}\text{C}$ (air was used as the oxidant gas) [29], which is comparable to our result considering the electrolyte thickness and oxidant gas. However, the power density obtained in this study is still lower than those of the cells using Ni-cermet anode [33,39]. Savaniu et al. [16] reported the performance of a cell with porous LST impregnated with GDC and Cu. They reported that the power density exceeded 500 mW cm^{-2} at 750 $^{\circ}\text{C}$ for the cell with 50–75 μm YSZ electrolyte. The results indicate that the performance of the cells with LST anode can be further improved by the cell design and optimization of cell components. For example, the ohmic resistance can be clearly decreased by decreasing the thickness and porosity of LSGM electrolyte. However, for LSGM electrolyte, the chemical stability between anode and electrolyte should be considered.

Fig. 15 shows the impedance spectra of the cells obtained at different temperatures. The ohmic resistance can be estimated from these spectra by the high frequency intercept with the abscissa. For the two types of cells (with the as-sprayed anode and annealed anode), when they operate at the same temperature, the real-axis intercepts at high frequency are almost at the same value. Because the fuel cells were assembled with the same electrolyte and cathode, the ohmic losses mainly arise from the electrolyte. For example, at 800 $^{\circ}\text{C}$, the ohmic resistance is $\sim 0.38 \Omega \text{ cm}^2$, consistent with the ohmic resistance expected for 300- μm thickness LSGM electrolytes [3]. However, a significant difference in the non-ohmic impedance was observed for the two types of cells. At 800 $^{\circ}\text{C}$, the non-ohmic impedances of ~ 1.13 and $0.73 \Omega \text{ cm}^2$ were observed in the cells with the as-sprayed anode (Fig. 15(a)) and annealed anode

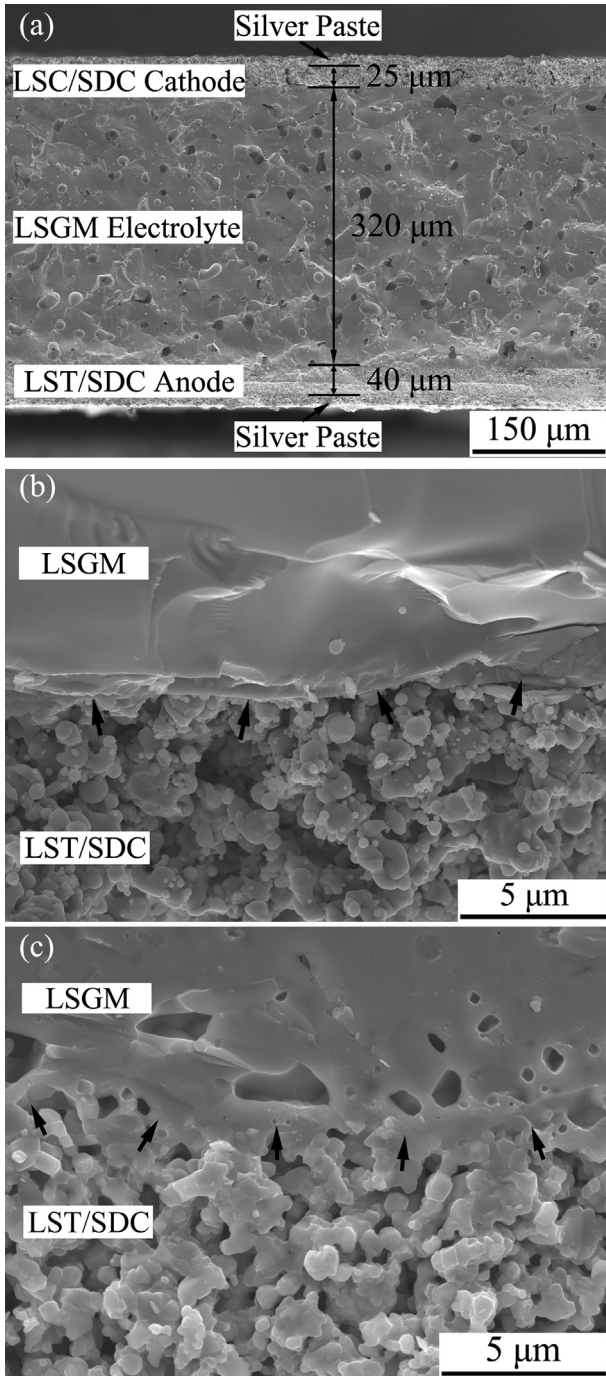


Fig. 13. (a) Cross section of the fractured SOFC single cell, (b) microstructure of the interface between the LST-SDC (as-sprayed) and LSGM, (c) microstructure of the interface between LST-SDC (annealed) and LSGM.

(Fig. 15(b)), respectively. The electrochemical impedance is a combination of anode and cathode impedances. Because the cells were made from the same electrolyte and cathode, therefore, the low non-ohmic impedance of the cell with the annealed anode can be attributed to the fact that the anode polarization resistance of the annealed anode is lower than the as-sprayed anode. As mentioned above, a relatively weak interface bonding was observed between the as-sprayed anode and electrolyte, and the cohesion of the particles in the anode was also weak. Horita et al. reported a cathode impedance of $\sim 0.2 \Omega \text{ cm}^2$ at 800 °C for the LSC-SDC composite cathode prepared by slurry coating [40].

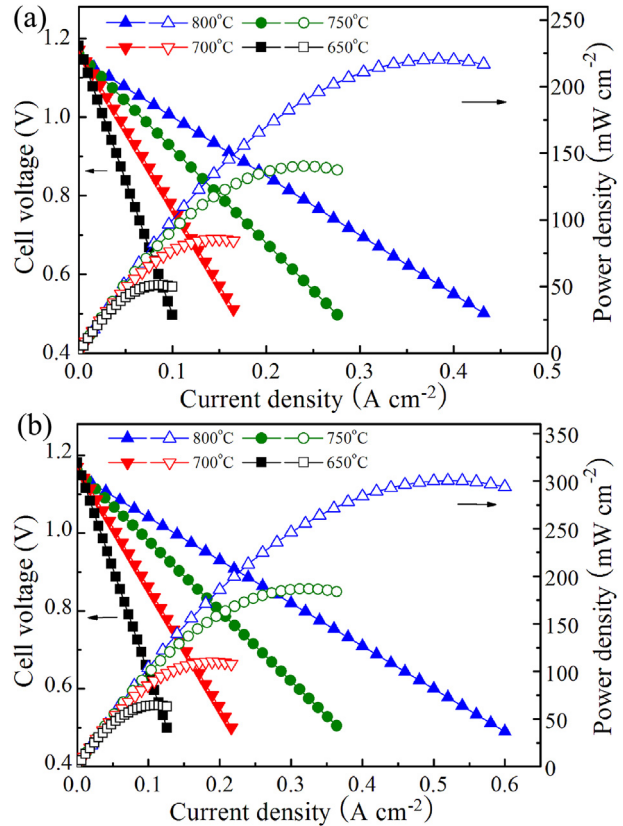


Fig. 14. Output performance of the single cell: (a) with the as-sprayed anode and (b) with the annealed anode.

Considering this value, it can be estimated that the anode impedance for the as-sprayed and annealed LST-SDC anodes in this study are ~ 0.93 and $0.53 \Omega \text{ cm}^2$ at 800 °C, respectively.

The corresponding Arrhenius plots of the cell polarization resistances determined from the EIS testing for the cells at OCV are shown in Fig. 16. The polarization resistance values (R_p) are much higher than the ohmic resistance values (R_{ohm}). The activation energy of the R_{ohm} of the cells was found to be ~ 0.62 eV. Because this value is similar to the values reported in the literature for bulk LSGM [41], clearly the R_{ohm} value is mostly determined by the

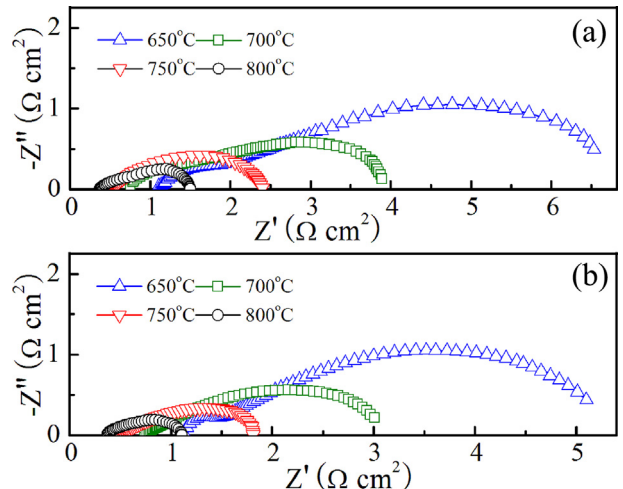


Fig. 15. Impedance spectra obtained for the cells under OCV conditions: (a) with the as-sprayed LST-SDC anode and (b) with the annealed LST-SDC anode.

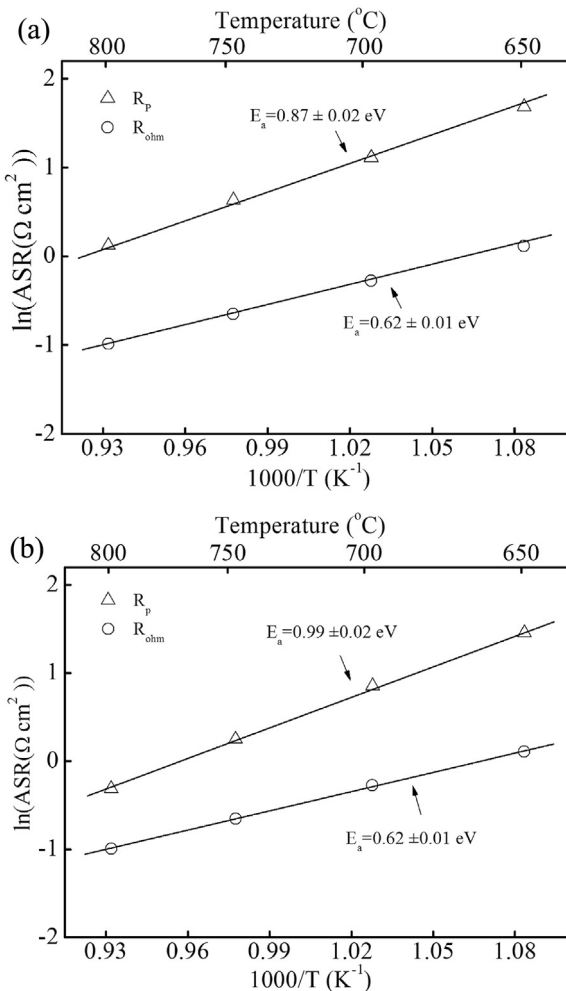


Fig. 16. Arrhenius plots of the polarization resistances for the cells: (a) with the as-sprayed LST–SDC anode and (b) with the annealed LST–SDC anode.

resistance of LSGM electrolyte. Moreover, the cell with the as-sprayed anode showed lower activation energy (0.87 eV) of R_p than the cell with the annealed anode (0.99 eV). With the annealed anode, although the interface bonding between the anode and electrolyte was improved, the particle size of the anode was increased, which would decrease the specific interface area for anode reaction. Moreover, the grain size of the particles in the anode was also increased after the annealing. Therefore, the activation energy of the anode can be increased by annealing.

4. Conclusions

In this study, nano-sized LST and SDC powders, suitable for use in SPS, were synthesized by sol–gel and glycine–nitrate processes, respectively. The study on the chemical stability of the conventional Ni anode and LSGM electrolyte showed that Ni reacts with LSGM electrolyte even at 600 °C. However, the results indicate that LST has a good chemical stability with LSGM and SDC electrolyte materials at high temperatures and in different atmospheres. Moreover, the LST–SDC composite anode fabricated by SPS showed the same phase structure as the original powders. The measurement afforded a porosity of ~40% for the as-sprayed anode. Moreover, the annealing conditions significantly affected the microstructure of anode deposit. The annealing causes the aggregation of particles by sintering, thus enhancing (i) the bonding between the particles

in the anode and (ii) the interface bonding between the anode and electrolyte. In the cell with 320-μm LSGM electrolyte and the as-sprayed LST–SDC anodes, the test afforded a maximum power density of 221 mW cm⁻² at 800 °C. After the anode was annealed at 1250 °C for 5 h, the power density of the cell increased by a factor of ~37% and reached 301 mW cm⁻² at 800 °C. The results indicate that the SPSed LST–SDC composite anode is promising for IT-SOFCs with LSGM electrolyte.

Acknowledgments

The present study is partially supported by National Basic Research Program (Grant No. 2012CB625100).

References

- [1] S.C. Singhal, K. Kendall, *High Temperature Solid Oxide Fuel Cells: Fundamentals, Design and Application*, Elsevier, 2004.
- [2] J.P.P. Huijsmans, F.P.F. van Berkel, G.M. Christie, *J. Power Sources* 71 (1998) 107–110.
- [3] T. Ishihara, *J. Am. Chem. Soc.* 116 (1994) 3801–3803.
- [4] M. Feng, J.B. Goodenough, *Eur. J. Solid State Inorg. Chem. T31* (1994) 663–672.
- [5] I. Minoru, M. Atsushi, *Solid State Ionics* 104 (1997) 303–310.
- [6] X. Zhang, S. Ohara, R. Maric, K. Mukai, T. Fukui, H. Yoshida, M. Nishimura, T. Inagaki, K. Miura, *J. Power Sources* 83 (1999) 170–177.
- [7] J.H. Joo, D.Y. Kim, G.M. Choi, *Solid State Ionics* 192 (2011) 523–526.
- [8] P. Huang, A. Horky, A. Petric, *J. Am. Ceram. Soc.* 82 (1999) 2402–2406.
- [9] T. Inagaki, K. Miura, H. Yoshida, R. Maric, S. Ohara, X. Zhang, K. Mukai, T. Fukui, *J. Power Sources* 86 (2000) 347–351.
- [10] C.H. Wang, C.H. Tsai, C.H. Lo, C.H. Sun, *J. Power Sources* 180 (2008) 132–142.
- [11] O.A. Marina, N.L. Canfield, J.W. Stevenson, *Solid State Ionics* 149 (2002) 21–28.
- [12] H.P. He, Y.Y. Huang, J.M. Vohs, R.J. Gorte, *Solid State Ionics* 175 (2004) 171–176.
- [13] X.F. Sun, R.S. Guo, J. Li, *Ceram. Int.* 34 (2008) 219–223.
- [14] T. Kolodiaznyi, A. Petric, *J. Electroceram.* 15 (2005) 5–11.
- [15] R. Mukundan, E.L. Brosha, F.H. Garzon, *Electrochim. Solid-State Lett.* 7 (2004) A5–A7.
- [16] C.D. Savaniu, J.T.S. Irvine, *Solid State Ionics* 192 (2011) 491–493.
- [17] K.B. Yoo, B.H. Park, G.M. Choi, *Solid State Ionics* 225 (2012) 104–107.
- [18] B.K. Park, J.W. Lee, S.B. Lee, T.H. Lim, S.J. Park, R.H. Song, W.B. Im, D.R. Shin, *Int. J. Hydrogen Energy* 37 (2012) 4319–4327.
- [19] F. Yi, H. Li, H. Chen, R. Zhao, X. Jiang, *Ceram. Int.* 39 (2013) 347–352.
- [20] R. Chiba, F. Yoshimura, Y. Sakurai, Y. Tabata, M. Arakawa, *Solid State Ionics* 175 (2004) 23–27.
- [21] H. Moon, S.D. Kim, E.W. Park, S.H. Hyun, H.S. Kim, *Int. J. Hydrogen Energy* 33 (2008) 2826–2833.
- [22] M.R. Somalu, V. Yufit, N.P. Brandon, *Int. J. Hydrogen Energy* 38 (2013) 9500–9510.
- [23] C.X. Li, C.J. Li, L.J. Guo, *Int. J. Hydrogen Energy* 35 (2010) 2964–2969.
- [24] O. Kwon, S. Kumar, S. Park, C. Lee, *J. Power Sources* 171 (2007) 441–447.
- [25] Y.C. Yang, Y.C. Chen, *J. Eur. Ceram. Soc.* 31 (2011) 3109–3118.
- [26] P. Fauchais, R. Etchart-Salas, C. Delbos, M. Tognoni, V. Rat, J.F. Coudert, T. Chartier, *J. Phys. D Appl. Phys.* 40 (2007) 2394–2406.
- [27] S. Ohara, R. Maric, X. Zhang, K. Mukai, T. Fukui, H. Yoshida, T. Inagaki, K. Miura, *J. Power Sources* 86 (2000) 455–458.
- [28] K.N. Kim, B.K. Kim, J.W. Son, J. Kim, H.W. Lee, J.H. Lee, J. Moon, *Solid State Ionics* 177 (2006) 2155–2158.
- [29] K.B. Yoo, G.M. Choi, *Solid State Ionics* 180 (2009) 867–871.
- [30] M. Kawano, H. Yoshida, K. Hashino, H. Ijichi, S. Suda, K. Kawahara, T. Inagaki, *J. Power Sources* 173 (2007) 45–52.
- [31] M. Kawano, H. Yoshida, K. Hashino, H. Ijichi, S. Suda, K. Kawahara, T. Inagaki, *Solid State Ionics* 177 (2006) 3315–3321.
- [32] S. Suda, S. Takahashi, M. Kawano, H. Yoshida, T. Inagaki, *Solid State Ionics* 177 (2006) 1219–1225.
- [33] T. Ishihara, H. Eto, J. Yan, *Int. J. Hydrogen Energy* 36 (2011) 1862–1867.
- [34] J. Fazilleau, C. Delbos, V. Rat, J.F. Coudert, P. Fauchais, B. Pateyron, *Plasma Chem. Plasma Process.* 26 (2006) 371–391.
- [35] C. Delbos, J. Fazilleau, V. Rat, J.F. Coudert, P. Fauchais, B. Pateyron, *Plasma Chem. Plasma Process.* 26 (2006) 393–414.
- [36] P. Datta, P. Majewski, F. Aldinger, *Mater. Chem. Phys.* 102 (2007) 240–244.
- [37] R. Polini, A. Pamio, E. Traversa, *J. Eur. Ceram. Soc.* 24 (2004) 1365–1370.
- [38] X. Sun, S. Wang, Z. Wang, X. Ye, T. Wen, F. Huang, *J. Power Sources* 183 (2008) 114–117.
- [39] S. Wang, M. Ando, T. Ishihara, Y. Takita, *Solid State Ionics* 174 (2004) 49–55.
- [40] Teruhisa Horita, Katsuhiko Yamaji, Natsuko Sakai, Harumi Yokokawa, A. Weber, E. Ivers-Tiffé, *Electrochim. Acta* 46 (2001) 1837–1845.
- [41] J.Y. Yi, G.M. Choi, *J. Eur. Ceram. Soc.* 24 (2004) 1359–1363.